THE ASTROPHYSICAL JOURNAL, 473:519–532, 1996 December 10


# ANOMALOUS CORONAL NEON ABUNDANCES IN QUIESCENT SOLAR ACTIVE REGIONS

J. T. SCHMELZ[1,2], J. L. R. SABA[3], D. GHOSH[2], AND K. T. STRONG[4]

*Received 1995 September 25; accepted 1996 June 27*

## ABSTRACT

The systematic differences between the solar photospheric and coronal composition are generally thought to be related to the first ionization potential (FIP) of the trace elements. While there are ample data showing that this is a significant factor, there is a growing body of observational evidence that a simple, FIP-based formula is not the whole story for coronal abundances. One of the most troubling problems for the FIP-based models is the apparent abundance variation of high-FIP (>11 eV) elements with respect to one another. We describe abundance variations of (high-FIP) neon relative to (high-FIP) oxygen, and (low-FIP) iron and magnesium, in solar active region observations made by the Flat Crystal Spectrometer on the *Solar Maximum Mission.* We show that, even in quiescent active regions, Ne/O can vary inconsistently with simple empirical FIP models: it shows values about a factor of 2 both above and below the "standard" coronal value of 0.15 obtained from solar energetic particle measurements of long-duration events (Reames). McKenzie & Feldman have recently invoked photoionization of O I by EUV radiation to explain *low* measurements of the Ne/O abundance ratio. Photoionization by a long-lived bath of soft X-rays and chromospheric evaporation have been suggested as being responsible for the anomalous behavior of neon in flares, but flare conditions should not apply in the quiescent regions of the present study. A complex picture involving the detailed dynamics, geometry, and radiation environment in the differentiation layer(s) may be required to understand coronal composition and its variability.

*Subject headings:* Sun: abundances — Sun: activity — Sun: corona

## 1. INTRODUCTION

Different sets of elemental abundances seem to characterize coronal and photospheric plasmas in the solar atmosphere. In situ solar wind and solar energetic particle (SEP) measurements, as well as spectroscopic observations, indicate that the first ionization potential (FIP) of the element is the dominant factor in determining how the coronal abundance will differ from its photospheric counterpart (Breneman & Stone 1985; Meyer 1985a, 1985b). These results suggest a mechanism (or mechanisms) operating in the chromosphere, at a temperature less than $10^4$ K, where the low-FIP elements are essentially ionized while the high-FIP elements remain largely neutral (see, e.g., Arnaud & Rothenflug 1985). Mechanisms have been proposed which increase the access of ions to the corona in order to explain an enhancement of low-FIP (<10 eV) elements with respect to their photospheric values. These models could explain the spectroscopic observations summarized by Feldman (1992) and the SEP results determined by Reames (1995). On the other hand, a mechanism which hinders the access of neutrals to the corona could explain a depletion of high-FIP (>11 eV) elements such as those reported by Veck & Parkinson (1982) and Fludra & Schmelz (1995).

It is possible that the coronal composition represents both a low-FIP enhancement *and* a high-FIP depletion, or that all elements are enhanced or all depleted, but by different relative amounts depending on FIP. At issue is the behavior of the heavy elements relative to hydrogen, which constitutes the bulk of the plasma. Analysis involving hydrogen is problematic in both the spectroscopic and SEP determinations of coronal abundances. In addition, there is disagreement between the spectroscopic measurements where normalization with respect to hydrogen is possible, at least in principle. The strongest evidence to date for correct normalization comes from the SEP analysis of Reames (1995) who finds that the abundances of low-FIP elements are enhanced above their photospheric values by about a factor of 3 and the abundances of high-FIP elements (other than helium and argon) are about 25% lower in the corona than in the photosphere. These results are usually taken as being consistent with the scenario where low-FIP elements are enhanced and high-FIP elements are the same in the photosphere and corona.

A strict interpretation of the empirical model based on the SEP results would predict no statistically significant coronal abundance variations. However, since such variations are observed, attempts have been made to explain them. Secondary effects like chromospheric evaporation and soft X-ray photoionization have been invoked to explain abundance anomalies in flares, where energetic bulk motions and high-energy photons are commonplace. But these models cannot work for quiescent active regions, under conditions where chromospheric evaporation and photoionization should not be factors. McKenzie & Feldman (1994) have argued that photoionization by blackbody radiation from just below the temperature minimum region, by locally produced Ly$\alpha$ radiation, and by line and continuum radiation at high temperatures, plays an important role in determining the chromospheric ionization structure. In particular, they suggest that photoionization of O I (and other high-FIP elements which have FIP<13.6 eV, the FIP of oxygen) by EUV radiation from above can shift the effective low-FIP/high-FIP boundary to higher

[1] University of Memphis, Physics Department, Memphis, TN 38152.
[2] Rhodes College, Physics Department, 2000 North Parkway, Memphis, TN 38112.
[3] Lockheed Solar and Astrophysics Group, NASA/GSFC Code 682, Greenbelt, MD 20771
[4] Lockheed Solar and Astrophysics Group, 3251 Hanover Street, Palo Alto, CA 94304.

TABLE 1

SPECTROSCOPIC TEMPERATURE ANALYSIS

| Number (1) | Date (2) | Time (UT) (3) | AR (4) | $T_e$[a](MK) (5) | $T_e$[b](MK) (6) | Fe XVIII (7) | Ca counts (8) | Ca spectra (9) | *GOES* (10) | Neon[c] (11) |
|---|---|---|---|---|---|---|---|---|---|---|
| 1........ | 1986 May 20 | 00:19–01:12 | 4729 | $2.66^{+0.16}_{-0.26}$ | $3.09^{+0.26}_{-0.34}$ | No | 7 | No | A5 | Ne/O high |
| 2........ | 1986 May 21 | 14:02–14:55 | 4731 | $2.92^{+0.07}_{-0.07}$ | $3.51^{+0.12}_{-0.12}$ | Low | 3 | No | A9 | Low |
| 3........ | 1986 May 23 | 02:11–03:07 | 4731 | $2.82^{+0.10}_{-0.10}$ | $3.35^{+0.16}_{-0.19}$ | Low | 4 | No | A5 | Low |
| 4........ | 1986 May 24 | 04:54–05:50 | 4731 | $2.88^{+0.07}_{-0.10}$ | $3.47^{+0.12}_{-0.19}$ | Low | 3 | No | A8* | Low |
| 5........ | 1987 Apr 11 | 22:26–23:21 | 4787 | $2.95^{+0.10}_{-0.07}$ | $3.59^{+0.17}_{-0.16}$ | Low | 6 | No | B7* | Std |
| 6........ | 1987 Apr 13 | 01:08–02:03 | 4787/90 | $3.09^{+0.04}_{-0.07}$ | $3.80^{+0.13}_{-0.13}$ | Med | 5 | No | B3* | Std |
| 7........ | 1987 Apr 14 | 14:50–15:45 | 4787/90 | $3.05^{+0.07}_{-0.07}$ | $3.76^{+0.09}_{-0.13}$ | Low | 4 | No | B2 | Std |
| 8........ | 1987 Apr 15 | 15:58–16:54 | 4787/90 | $3.47^{+0.04}_{-0.04}$ | $4.52^{+0.11}_{-0.10}$ | High | 40 | Yes | B4 | Ne/O std* |
| 9........ | 1987 Apr 15 | 23:22–24:17 | 4787/90 | $3.05^{+0.07}_{-0.07}$ | $3.76^{+0.13}_{-0.13}$ | High | 14 | Yes | B3* | Ne/O std* |
| 10 ...... | 1987 Apr 19 | 14:41–15:10 | 4787/90 | $3.09^{+0.04}_{-0.07}$ | $3.85^{+0.09}_{-0.13}$ | Med | 57 | Yes | C2* | Std |
| 11 ...... | 1987 May 26 | 01:12–02:08 | 4811 | $3.59^{+0.08}_{-0.08}$ | $4.73^{+0.17}_{-0.16}$ | High | 56 | Yes | C2* | Ne/O high* |
| 12 ...... | 1987 May 29 | 18:43–19:39 | 4811 | $3.02^{+0.18}_{-0.33}$ | $3.72^{+0.31}_{-0.55}$ | No | 13 | Yes | B4* | Ne/O high |
| 13 ...... | 1987 Jun 13 | 02:40–03:36 | SN50 | $2.75^{+0.16}_{-0.24}$ | $3.27^{+0.23}_{-0.36}$ | No | 3 | No | B1 | Low |
| 14 ...... | 1987 Nov 27 | 16:20–17:17 | 4891 | $2.79^{+0.06}_{-0.13}$ | $3.27^{+0.15}_{-0.18}$ | No | 4 | No | B2 | Low |
| 15 ...... | 1987 Nov 29 | 20:07–21:06 | 4891 | $2.88^{+0.07}_{-0.07}$ | $3.47^{+0.12}_{-0.12}$ | No | 7 | No | B2 | Ne/O std |
| 16 ...... | 1987 Dec 06 | 16:58–18:01 | 4901 | $3.43^{+0.12}_{-0.08}$ | $4.47^{+0.16}_{-0.15}$ | High | 7 | Yes? | B2* | ?* |
| 17 ...... | 1987 Dec 07 | 10:15–11:17 | 4901 | $2.92^{+0.10}_{-0.10}$ | $3.55^{+0.17}_{-0.20}$ | No | NA | NA | B1 | Ne/O high |
| 18 ...... | 1987 Dec 07 | 14:48–16:01 | 4901 | $2.99^{+0.10}_{-0.13}$ | $3.63^{+0.17}_{-0.20}$ | Low | NA | NA | B1 | Ne/O high |
| 19 ...... | 1987 Dec 08 | 03:32–04:34 | 4901 | $2.72^{+0.19}_{-0.46}$ | $3.16^{+0.35}_{-0.59}$ | No | NA | NA | B1 | Ne/O high |
| 20 ...... | 1987 Dec 08 | 09:49–10:51 | 4901 | $3.20^{+0.07}_{-0.11}$ | $4.03^{+0.14}_{-0.18}$ | No | NA | NA | B2* | Ne/O high |
| 21 ...... | 1987 Dec 08 | 16:06–17:08 | 4901 | $3.05^{+0.07}_{-0.14}$ | $3.76^{+0.18}_{-0.21}$ | Low | NA | NA | B2 | Ne/O high |
| 22 ...... | 1987 Dec 09 | 03:06–04:08 | 4901 | $3.13^{+0.07}_{-0.04}$ | $3.94^{+0.09}_{-0.13}$ | Low | NA | NA | B3 | ? |
| 23 ...... | 1987 Dec 09 | 07:48–08:50 | 4901 | $2.02^{+0.55}_{-0.43}$ | $2.26^{+0.69}_{-0.68}$ | No | NA | NA | B2* | Ne/O high |
| 24 ...... | 1987 Dec 10 | 02:39–03:40 | 4901 | $3.02^{+0.11}_{-0.14}$ | $3.72^{+0.18}_{-0.25}$ | No | NA | NA | B3 | Ne/O high |
| 25 ...... | 1987 Dec 10 | 10:31–11:31 | 4901 | $2.79^{+0.20}_{-0.39}$ | $3.31^{+0.32}_{-0.56}$ | No | NA | NA | B1 | Ne/O high |
| 26 ...... | 1987 Dec 11 | 02:13–03:13 | 4901 | $3.05^{+0.07}_{-0.03}$ | $3.80^{+0.09}_{-0.09}$ | Low | 3 | No | B9 | ? |
| 27 ...... | 1987 Dec 11 | 10:04–11:04 | 4901 | $3.24^{+0.08}_{-0.04}$ | $4.12^{+0.10}_{-0.09}$ | High | 6 | Yes? | B4 | ?* |
| 28 ...... | 1987 Dec 13 | 09:10–10:09 | SELimb | $2.79^{+0.10}_{-0.09}$ | $3.31^{+0.16}_{-0.15}$ | No | 5 | No | B2 | Std |
| 29 ...... | 1987 Dec 15 | 03:34–04:31 | 4906 | $3.02^{+0.07}_{-0.07}$ | $3.72^{+0.13}_{-0.17}$ | No | 5 | Yes | B4* | Std |
| 30 ...... | 1987 Dec 16 | 07:49–08:46 | 4906 | $3.09^{+0.07}_{-0.10}$ | $3.80^{+0.13}_{-0.13}$ | No | 5 | No | B2 | Std |
| 31 ...... | 1987 Dec 18 | 03:46–04:42 | 4906 | $2.54^{+0.21}_{-0.68}$ | $2.95^{+0.28}_{-0.96}$ | No | 4 | No | B1 | Ne/O low |
| 32 ...... | 1987 Dec 18 | 06:54–07:50 | 4906 | $2.92^{+0.28}_{-0.33}$ | $3.51^{+0.52}_{-0.92}$ | No | 5 | No | B1 | Ne/O low |
| 33 ...... | 1987 Dec 20 | 09:07–10:03 | 4906 | $3.72^{+0.27}_{-0.48}$ | $4.95^{+0.67}_{-0.88}$ | No | NA | NA | 29 | Std |

[a] Uses the ionization balance calculations of Arnaud & Rothenflug 1985.

[b] Uses the ionization balance calculations of Arnaud & Raymond 1992.

[c] Most entries describe neon abundance compared with oxygen, magnesium, and iron. When results were not clear, we state Ne/O only. A question mark indicates that the emission measure-temperature plots were inconclusive, while an asterisk means that there was strong evidence of hot material in the FCS field of view.

FIP values, and thus account for variations in the Ne/O abundance ratio. However, this mechanism can produce only anomalously *low* values of Ne/O (by enhancing oxygen, but not depleting neon), not *enhanced* Ne/O.

In this paper, we analyze spectral data from quiescent active regions, with emphasis on the coronal abundance of the element neon. Since neon has the highest FIP of any element except helium, an empirical model based on the SEP results would predict that the abundance of neon, relative to hydrogen or to any of the other high-FIP elements, is the same in the photosphere and corona and, in the absence of flare-related effects like chromospheric evaporation and photoionization, should show no abundance variations. Our data, however, show evidence that the coronal abundance of neon can vary from one active region measurement to another. These variations include depletions of Ne/O, as reported by McKenzie & Feldman (1992) from SOLEX data and explained as being due to oxygen enhancements (McKenzie & Feldman 1994). However, we also find depletions of neon relative to oxygen, magnesium, and iron, which seems to imply variations in the absolute neon abundance itself as well as *enhancements* of Ne/O above the benchmark coronal value of 0.15 determined from SEP measurements of long-duration events (Reames 1995). Depletions of neon or enhancements of Ne/O have not yet been explained by models seeking to predict coronal abundances in quiescent regions.

## 2. OBSERVATIONS

The spectra used in this study are from the *Solar Maximum Mission* (*SMM*) Flat Crystal Spectrometer (FCS; Acton et al. 1980), which had a field of view of about 15 arcsec (FWHM) and could scan the soft X-ray resonance lines of prominent ions in the spectral range of 1.5–20.0 Å. These lines are sensitive to a broad range of plasma temperatures (1.5–50 MK) and can be used to determine temperature, emission measure, density, and relative elemental abundances. (Since the FCS continuum is dominated by nonsolar background, and, in any case, the actual solar continuum includes a large free-bound component at active region temperatures, it is not possible to obtain absolute abundances from FCS line-to-continuum measurements). The FCS observing sequence used to accumulate the spectra analyzed in this study started with a low-resolution image of the active region. The instrument was then pointed at the brightest pixel of that image and began a spectroscopic scan at about 13 Å. It continued scanning at a rate of about 0.01 Å $s^{-1}$ to 19 Å. This spectral range covers bright resonance lines of Ne IX (13.45 Å), Fe XVIII (14.22 Å), Fe XVII (16.78 Å), and O VIII (18.97 Å) which were used in this study. In a higher energy FCS channel, the range of 7.3–9.5 Å was scanned simultaneously. The Mg XI (9.17 Å) resonance line, covered in this second channel, was also used here. Upper limits on high-temperature lines scanned in various FCS channels were used to constrain the amount of high-temperature plasma in the FCS field of view. Covering the full wavelength range took approximately 10 minutes. In general, four to five of these spectroscopic scans were done during the daylight portion of the 90 minute *SMM* orbit. For details of the spectral fitting procedure, see Saba & Strong (1991).

The analysis presented here is limited to those spectra obtained from several active regions during quiescent periods (see Table 1). Spectra taken during flares and long-duration events were deliberately excluded from the sample to eliminate physical conditions which changed with time. Several criteria had to be met for a spectrum to be included in the sample. For example, the background and the fluxes of the various spectral lines could not vary significantly (i.e., $\geq 15\%$) from scan to scan within a given orbit, and the count rate in the Ca XVIII–XIX channel of the *SMM* Bent Crystal Spectrometer (BCS) could not be greater than 60 counts per second (an arbitrary "flare" cutoff). Of the 75 FCS long spectral scan data sets available, 33 met these criteria and are listed in Table 1. An additional screening, discussed in § 3.3, was used to exclude five of these spectra which showed evidence of hot plasma. The remaining 28 spectra were used in this analysis. For these active region spectra, the plasma emitting the spectral lines observed by the FCS may be considered *effectively* isothermal. That is, the plasma emission to which the FCS was sensitive could not be distinguished from isothermal emission, within measurement uncertainties. This assumption is discussed in detail in § 3.3 below.

In this paper, we assume initially the "adopted" coronal abundances of Meyer (1985b) for oxygen, neon, and magnesium: $O/H = 2.34 \pm 0.71 \times 10^{-4}$, $Ne/H = 3.55 \pm 0.91 \times 10^{-5}$, and $Mg/H = 3.80 \pm 0.18 \times 10^{-5}$ and, for iron, both the "photospheric" $Fe/H = 4.68 \pm 0.33 \times 10^{-5}$ and the "meteoritic" $Fe/H = 3.23 \pm 0.08 \times 10^{-5}$ values from Grevesse & Anders (1989). We compare our results with these "standard" values.

## 3. ANALYSIS

### 3.1. *Evidence of Neon Abundance Variations*

Striking differences in the FCS active region spectra, such as those shown in Figure 1, motivated the original FCS abundance investigations by Strong et al. (1988, 1991). Figures 1*a* and 1*b* compare the count rates as a function of wavelength for a portion of the spectra acquired for two quiescent active regions with approximately the same electron temperature (based on temperature diagnostic line

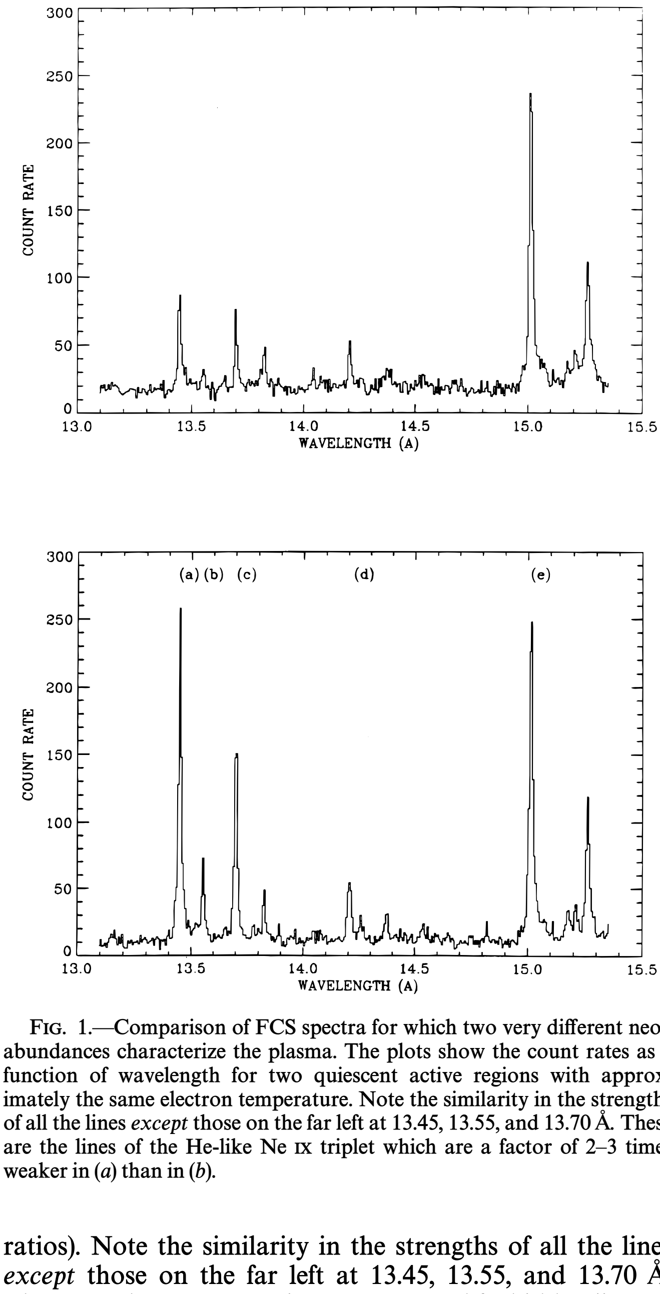


FIG. 1.—Comparison of FCS spectra for which two very different neon abundances characterize the plasma. The plots show the count rates as a function of wavelength for two quiescent active regions with approximately the same electron temperature. Note the similarity in the strengths of all the lines *except* those on the far left at 13.45, 13.55, and 13.70 Å. These are the lines of the He-like Ne IX triplet which are a factor of 2–3 times weaker in (*a*) than in (*b*).

ratios). Note the similarity in the strengths of all the lines *except* those on the far left at 13.45, 13.55, and 13.70 Å. These are the resonance, intersystem, and forbidden lines of the He-like Ne IX triplet. They are much weaker in Figure 1*a* than in Figure 1*b* relative to all the other lines, including the nearby weak Fe XVII line at 13.82 Å which was scanned within 30 s of the neon lines; the relative line strengths of the other lines remain approximately constant between the two spectra. One possible explanation for this dramatic difference is that the neon abundance of the plasma producing the spectrum in Figure 1*b* is a factor of approximately 2–3 higher than that producing the spectrum in Figure 1*a*. We show below that this is the most likely interpretation.

To investigate how widespread these potential neon abundance variations are, we first examine ratios of spectral lines with similar temperature sensitivities and look for variations that can be explained only in terms of abundance anomalies. This method requires a temperature diagnostic, usually a ratio of spectral lines emitted by the same element so the result is abundance-independent.

The photon flux $F$ measured at Earth of an optically thin spectral line emitted at the Sun under "coronal conditions" of low density and thermodynamic equilibrium is

$$F = C \times \int AG(T_e) n_e^2 \, dV \,, \tag{1}$$

where $C$ is a constant scaling factor, $A$ is the abundance with respect to hydrogen of the element producing the line, $G(T_e)$ is the emissivity function (a temperature-dependent term containing the excitation and ionization properties of the atom producing the line), $n_e$ is the electron density, and $dV$ is the volume element. If the temperature and abundance distribution are essentially constant for the plasma in the field of view which contributes to the line emission, then the $A$ and $G(T_e)$ factors can be pulled outside the integral:

$$F = CAG(T_e) \int n_e^2 \, dV \,, \tag{2}$$

where $\int n_e^2 \, dV$ is the familiar volume emission measure, $\mathrm{EM}_V$. The isothermal assumption, discussed in § 2, is justified in the discussion of Figure 3 below.

Here, the emissivity tabulations of Mewe, Gronenschild, & van den Oord (1985) are used to evaluate the $G(T_e)$ functions for the O VIII, Ne IX, and Mg XI lines. For the Fe XVII line, we use new results for the excitation rates from Bhatia & Doschek (1992). For the Fe XVIII blend at 14.22 Å, we use the calculation of McKenzie et al. (1992). For the non-iron lines, we assume the ionization balance results of Arnaud & Rothenflug (1985), while for the iron lines, we use both Arnaud & Rothenflug (1985) and Arnaud & Raymond (1992) for comparison.

To find the relative abundances for two optically thin lines emitted under "coronal conditions" of low density and thermodynamic equilibrium from the same volume of plasma, we take the ratio of the measured photon fluxes:

$$\frac{F_1}{F_2} = \frac{A_1 \, G_1(T_e)}{A_2 \, G_2(T_e)} \,. \tag{3}$$

If the ratio of the $G(T_e)$ functions is invariant or changes slowly with temperature in the relevant temperature regime (i.e., where there is significant contribution to one or both lines), then the photon flux ratio gives a direct measure of the relative abundances.

In earlier work (Strong et al. 1988, 1991; McKenzie & Feldman 1992; Saba & Strong 1992, 1993), the temperature diagnostic of choice has been the flux ratio of the Fe XVIII line at 14.22 Å to the Fe XVII line at 15.01 Å. This ratio is a strong function of temperature, varying by nearly 2 orders of magnitude over the range 2–4 MK. Further, the 15.01 Å line is the strongest line in the soft X-ray part of the spectrum at active region plasma temperatures and was, therefore, an obvious first choice. It may, however, be significantly affected by resonance scattering (Schmelz, Saba, & Strong 1992; Saba et al. 1997), with 15.01 Å photons from the centers of active regions being scattered preferentially out of the line of sight. In this case, the FCS would not observe the full line flux and the derived temperature would be too high. To avoid this possible problem, we use the flux ratio of the Fe XVIII line at 14.22 Å to the Fe XVII line at 16.78 Å as our temperature diagnostic. The 16.78 Å line is strong, with a relatively small statistical uncertainty, but also has a small oscillator strength, so that it should not be affected significantly by resonance scattering (the scattering opacity is about 4% that of the 15.01 Å line).

For other spectral lines in the FCS wavelength range, we find that the opacity effects are minimal and do not significantly affect the measured fluxes for these quiescent active region data (Schmelz et al. 1997). To find the electron temperature, assuming an isothermal approximation for the plasma, we take the ratio of the line fluxes:

$$\frac{F_{14.22}}{F_{16.78}} = \frac{A_{\mathrm{Fe}} \, G_{14.22}(T_e)}{A_{\mathrm{Fe}} \, G_{16.78}(T_e)} = \frac{G_{14.22}(T_e)}{G_{16.78}(T_e)} \Rightarrow T_e \,. \tag{4}$$

The line-ratio temperature analysis is done twice, once using the ionization balance calculations of Arnaud & Rothenflug (1985) for Fe XVII and Fe XVIII, and a second time using the results of the revised calculations by Arnaud & Raymond (1992). The resulting temperatures are listed in Table 1 where column (1) gives the running spectrum number, (2) the date of the FCS spectroscopic scan, (3) the time of the scan, (4) the NOAA active region number, (5) $T_e$ for the calculations of Arnaud & Rothenflug (1985), and (6) $T_e$ for the calculations of Arnaud & Raymond (1992). For all of the spectroscopic scans, the temperatures in column (6) are systematically higher than those in column (5), typically by 0.5 MK and even more for the hotter regions.

The results of this temperature analysis are used in Figure 2. In Figure 2*a* we plot the photon flux ratio of the Ne IX line to the Fe XVII line on the ordinate against the $\log_{10} T_e$ on the abscissa. The data from the 33 FCS spectra are plotted as crosses where the extent of the vertical line represents the $\pm 1\ \sigma$ statistical error on the measured photon flux ratio. The length of the horizontal crossbar represents the $\pm 1\ \sigma$ error on $T_e$ from equation (4); this results from the statistical uncertainty in the iron flux ratio and is typically $\pm 0.03$ on the log $T_e$ scale. The temperatures used are those listed in column (5) of Table 1, and the Arnaud & Rothenflug (1985) ionization balance calculations were used to produce the theoretical curves which run through the data. These curves predict how the photon flux ratio should vary as a function of temperature for a "standard" coronal abundance ratio of Ne/Fe = 0.75 for the "photospheric" abundance for iron (*solid line*) and 1.10 for the "meteoritic" value (*dashed line*) (Grevesse & Anders 1989). We repeat the process in Figure 2*b*, but use, instead, the temperatures listed in column (6) of Table 1 and the Arnaud & Raymond (1992) ionization fractions for iron to produce the theoretical predictions.

We compare these Ne/Fe results with those of O/Fe. The photon flux ratio of the O VIII line to the Fe XVII line is plotted on the ordinate of Figure 2*c* and Figure 2*d*. Figure 2*c* uses the ionization balance calculations of Arnaud & Rothenflug (1985) for both ions, while Figure 2*d* substitutes those of Arnaud & Raymond (1992) for iron. The solid lines again show the theoretical prediction of how the flux ratio should vary as a function of temperature for a "standard" coronal abundance ratio of O/Fe (5.00 for the "photospheric" abundance for iron or 7.24 for the "meteoritic" value—Grevesse & Anders 1989). Note that, no matter which iron abundance or ionization balance calculation is used, the scatter in the data perpendicular to the predicted curve is always greater for Ne/Fe than for O/Fe, suggesting that the neon abundance could be varying.

To examine this possibility, we plot, after Strong (1978), the curves of log $\mathrm{EM}_V$ against log $T_e$ for each line considered in our sample spectra. We use measured fluxes of four spectral lines of different elements, i.e., O VIII, Fe XVII,

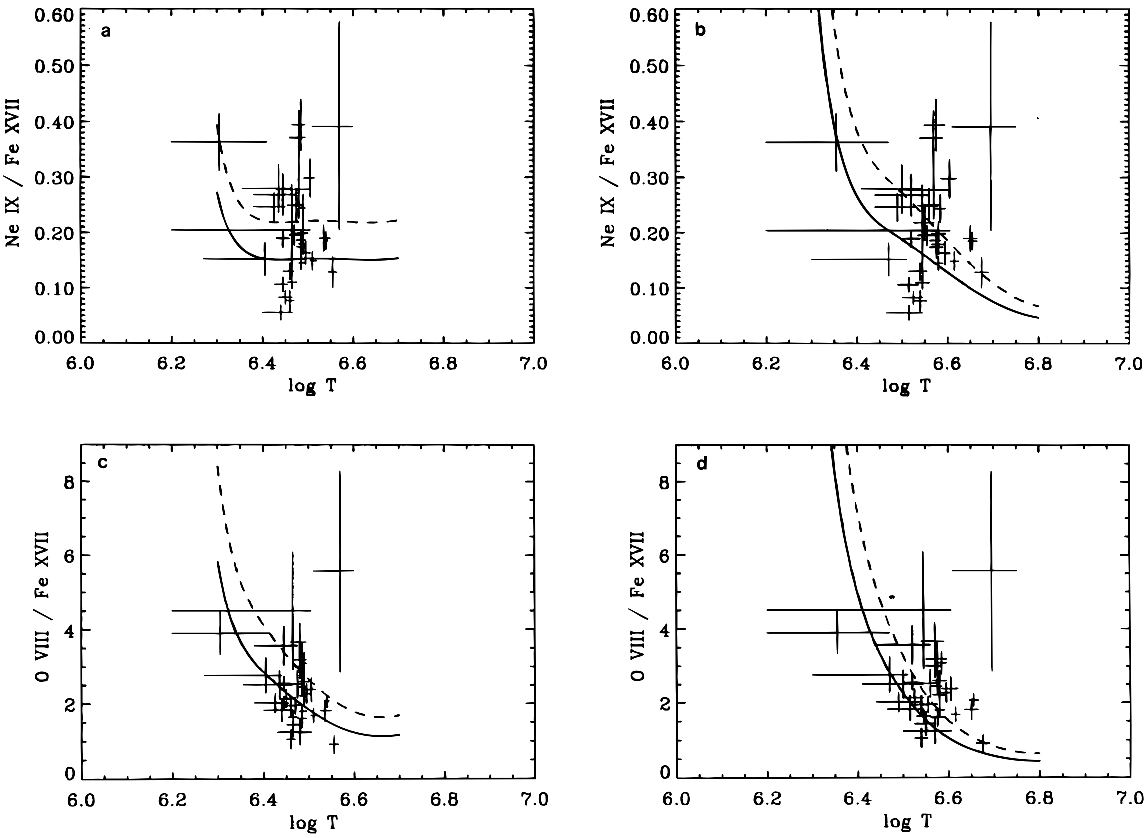


FIG. 2.—Comparison of Ne IX/Fe XVII and O VIII/Fe XVII flux ratios. The data from the FCS spectra are plotted as crosses where the extent of the vertical line represents the $\pm 1\ \sigma$ statistical error on the measured flux ratio. The length of the horizontal crossbar represents the $\pm 1\ \sigma$ error on the temperature from eq. (4). Figures 2*a* and 2*c* use the Arnaud & Rothenflug (1985) ionization balance calculations while Figs. 2*b* and 2*d* use those of Arnaud & Raymond (1992) for iron. The curves depict the theoretical flux ratio as a function of temperature for "standard" coronal abundance ratios of Ne/Fe = 0.75 and O/Fe = 5.00 for the "photospheric" abundance for iron (*solid line*) and Ne/Fe = 1.10 and O/Fe = 7.24 for the "meteoritic" value (*dashed line*).

Ne IX, and Mg XI, from the different spectra. The $EM_V(T_e)$ curve for a given spectral line is obtained by dividing the measured flux by its theoretical emissivity and an assumed elemental abundance (see eq. [2]). In Figure 3, we show six plots which illustrate our basic findings for neon. The bands for each line in the figure correspond to $\pm 1\ \sigma$ statistical uncertainties of the measured line flux where we have assumed the "standard" values of the elemental abundances listed in § 2 above. In the isothermal case, the intersection of the bands should give the jointly allowed $T_e$—$EM_V$ solution if the correct relative abundances are assumed. There is better agreement when the "photospheric" abundance for iron is used rather than the lower "meteoritic" value. (Note: If a different normalization of the elements with respect to hydrogen is preferred, the relative results do not change. The bands will simply scale up or down jointly in the plot, changing the absolute emission measure, but keeping the same temperature and relative $EM_V$ intersection as the plots in Fig. 3.)

Note that in Figure 3*a*, for the FCS spectrum (number 6 in Table 1) taken of NOAA AR 4787 on 1987 April 13, all four bands overlap near the center of the plot. From this result, we can be fairly confident that the plasma observed with FCS is well described by an electron temperature of $T_e = 3.21 \pm 0.05 \times 10^6$ K (log $T_e = 6.50$) and an emission measure of $EM_V = 1.78 \pm 0.04 \times 10^{47}$ cm$^{-3}$ (log $EM_V$ = 47.25), and that the relative elemental abundances are consistent with the standard set for the corona. Similarly for Figure 3*b*, FCS data (spectrum number 30) taken of AR 4906 on 1987 December 16 indicate an electron temperature of $T_e = 3.10 \pm 0.06 \times 10^6$ K (log $T_e = 6.49$) and an emission measure of $EM_V = 1.86 \pm 0.05 \times 10^{47}$ cm$^{-3}$ (log $EM_V = 47.27$). At least six other spectra in our sample (numbers 5, 7, 10, 28, 29, and 33 in Table 1) show a similar intersection with "standard" abundances.

Next, we look for deviations from this result. The emission measure versus temperature curves for the same four soft X-ray lines measured from the spectrum taken of SN 50 taken on 1987 June 13 (spectrum number 13) are plotted in Figure 3*c* and that of AR 4731 on 1986 May 23 in Figure 3*d* (spectrum number 3). These give a very different impression than the plots in Figure 3*a* and 3*b*. The O VIII, Fe XVII, and Mg XI bands intersect at temperatures of $T_e = 3.21 \pm 0.06 \times 10^6$ K (log $T_e = 6.50$) and $T_e = 3.31 \pm 0.06 \times 10^6$ K (log $T_e = 6.52$), respectively, and at emission measures of $EM_V = 1.74 \pm 0.05 \times 10^{47}$ cm$^{-3}$ (log $EM_V = 47.23$) and $EM_V = 1.66 \pm 0.05 \times 10^{47}$ cm$^{-3}$ (log $EM_V = 47.22$). In both cases, however, the Ne IX emission measure band is too low relative to the intersection of the other lines. The most straightforward explanation for this is that the "standard" neon abundance used to produce these plots is too high relative to oxygen, magnesium, and iron abundances. If we lower the abundance to Ne/H = $1.3 \times 10^{-5}$ $\pm 15\%$ in the case of SN 50 and Ne/H = $1.7 \times 10^{-5}$ $\pm 15\%$ in the case AR 4731, the Ne IX bands move up and intersect the other bands at the appropriate temperature and emission measure.

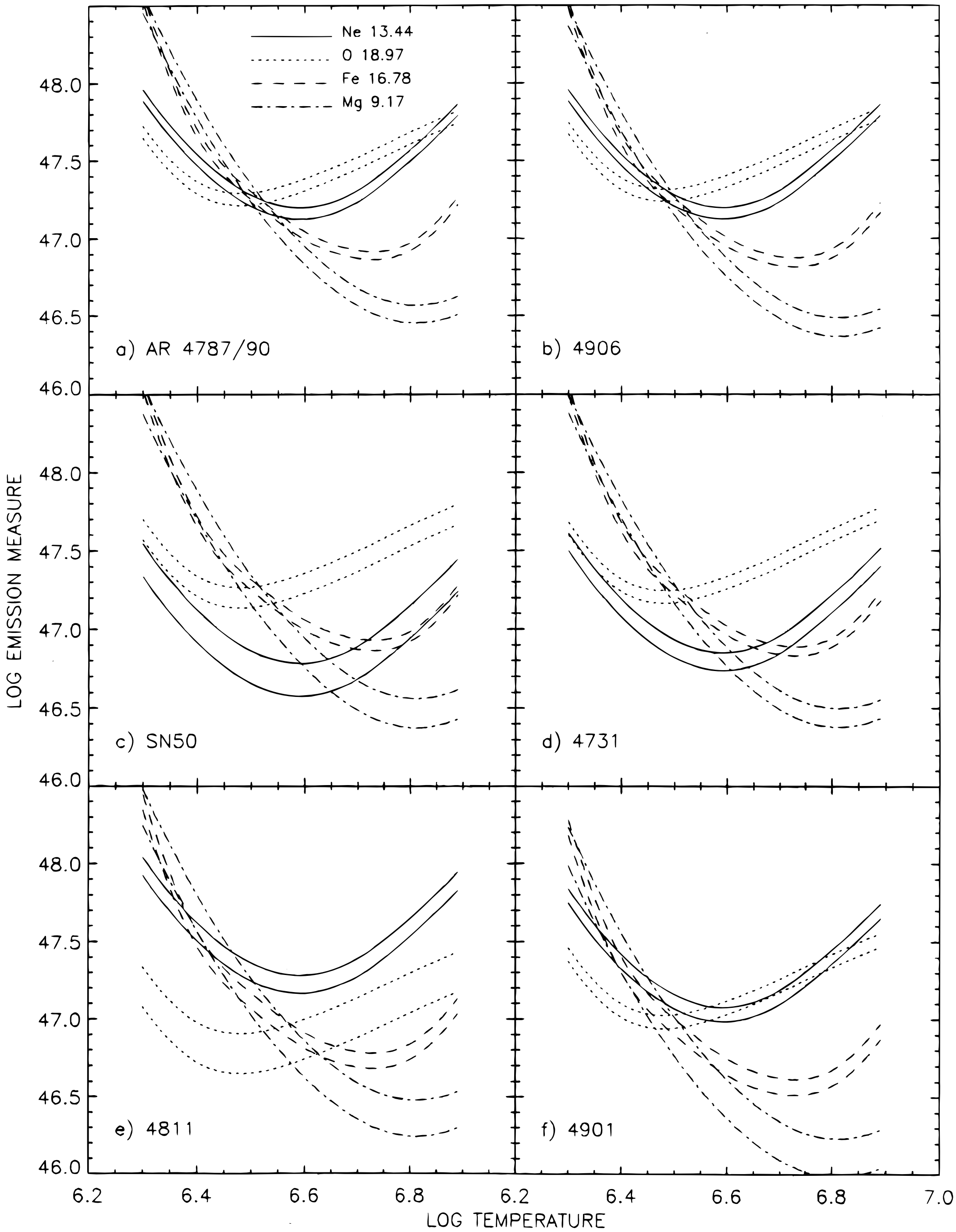


FIG. 3.—Emission measure vs. temperature plots obtained by dividing measured fluxes by predicted emissivities, after Strong (1978). The results for four spectral lines, i.e., O VIII, Fe XVII, Ne IX, and Mg XI, are plotted. The bands correspond to $\pm 1$ $\sigma$ statistical uncertainties in the measured line flux for "standard" coronal abundances O/H = $2.34 \times 10^{-4}$, Ne/H = $3.55 \times 10^{-5}$, and Mg/H = $3.80 \times 10^{-5}$, and Fe/H = $4.68 \times 10^{-5}$. For (*a*) AR 4787 on 1987 April 13 and (*b*) AR 4906 on 1987 December 16, all four bands overlap near the center of the plot at a single small region of electron temperature and emission measure, indicating that the elemental abundances are consistent with the standard set for the corona and the detected emission is effectively isothermal. For (*c*) SN 50 on 1987 June 13 and (*d*) AR 4731 on 1986 May 23, the O VIII, Fe XVII, and Mg XI bands intersect at a given temperature and emission measure but the Ne IX band is too low. If we lower the abundance to Ne/H = $1.3 \times 10^{-5}$ $\pm 15\%$ in the case of SN 50 and Ne/H = $1.7 \times 10^{-5}$ $\pm 15\%$ in the case of AR 4731, the neon bands move up and intersect the other bands at the appropriate temperature and emission measure region. For (*e*) AR 4811 on 1987 May 29 and (*f*) AR 4901 on 1987 December 8, the O VIII, Fe XVII, and Mg XI bands intersect but the Ne IX band is too high. If we raise the abundance to Ne/H = $7.5 \times 10^{-5}$ $\pm 15\%$ in the case of AR 4811 and Ne/H = $5.5 \times 10^{-5}$ $\pm 15\%$ in the case of AR 4901, the neon bands move down to intersect the other bands in the appropriate temperature and emission measure region.

Figure 3*e* (AR 4811 on 1987 May 29, spectrum number 12) and 3*f* (AR 4901 on 1987 December 8, spectrum number 20), once again, show the O VIII, Fe XVII, and Mg XI emission measure bands intersecting, at temperatures of $T_e = 3.54 \pm 0.07 \times 10^6$ K (log $T_e = 6.55$) and $T_e = 3.12 \pm 0.06 \times 10^6$ K (log $T_e = 6.49$), respectively, and at emission measures of $\mathrm{EM}_V = 9.33 \pm 0.06 \times 10^{46}$ cm$^{-3}$ (log $\mathrm{EM}_V = 46.97$) and $\mathrm{EM}_V = 9.77 \pm 0.05 \times 10^{46}$ cm$^{-3}$ (log $\mathrm{EM}_V = 49.99$). In both cases, however, the Ne IX band is too high, relative to the intersection of the other three bands indicating that the "standard" neon abundance used to produce these plots is too low. If we raise the abundance to $\mathrm{Ne/H} = 7.5 \times 10^{-5} \pm 15\%$ in the case of AR 4811 and $\mathrm{Ne/H} = 5.5 \times 10^{-5} \pm 15\%$ in the case of AR 4901, the neon bands move down to intersect the other bands at the appropriate temperature-emission measure region.

Note that the plots in Figures 3*e* and 3*f* could also indicate that the oxygen band is too low, rather than the neon band too high. In the case of AR 4901 (Fig. 3*f*, spectrum number 20), the line-ratio temperature analysis suggests that the higher temperature solution, which points to a variation in neon (relative to oxygen, magnesium, and iron), is preferred. The cooler solution, where the neon, iron, and magnesium emission measure bands intersect at approximately $T_e = 2.51 \times 10^6$ K ($\log T_e = 6.40$) is inconsistent with the temperature determined from the abundance-independent ratio of the Fe XVIII to the Fe XVII line fluxes for either ionization balance calculation. For AR 4811 (Fig. 3*e*, spectrum number 12), the ambiguity is not resolved by the temperature analysis. The intersection of the neon, iron, and magnesium bands agrees with the temperature determined using the ionization fractions of Arnaud & Rothenflug (1985), while the intersection of the oxygen, iron, and magnesium bands agrees with that determined using the ionization fractions of Arnaud & Raymond (1992). Nevertheless, in either case, the Ne/O abundance is significantly greater than 0.15, the "standard" value for the corona (e.g., Meyer 1985b; Reames 1995).

The plots in Figures 3*c*–3*f* depict the most extreme examples in our sample of neon (or Ne/O) abundance variations in active regions for which the other relative abundances are standard. However, we are not trying to imply these are the only kind of abundance variations. The $\mathrm{EM}_V$-$T_e$ plots for other active regions in our sample are sometimes more complex than those depicted in Figure 3, with only two of the four bands intersecting at any one point. This would indicate that the abundances of two or more of the elements have deviated from their "standard" coronal values or that the plasma is other than "effectively isothermal." The interpretation of such plots is more difficult than, for example, those in Figures 3*a* and 3*b*, and outside the scope of this paper. We have chosen the simplest plots to illustrate the main point of this paper, i.e., that the abundance of neon can vary and that the Ne/O abundance ratio can be enhanced or depleted, compared to the standard value of 0.15, even in quiescent active regions.

### 3.2. *Possible Explanations for Neon Flux Variations*

To verify that the results of Figures 1–3 imply neon or Ne/O abundance changes, other possible explanations that could affect the flux of the neon lines or the Ne IX/O VIII line ratios must be examined and eliminated.

1. The theoretical calculations for the excitation rates of one or more of the lines used in the study could be in error. However, three of the lines are relatively simple: O VIII is H-like and Ne IX and Mg XI are He-like. These lines are thought to be well understood because of their relative simplicity. The Fe XVII line, however, is more complex. It is Ne-like and the excitation rate calculations are much more difficult. Bhatia & Doschek (1992) have recently upgraded these calculations and we use these new results here. If there were a problem with the excitation rates, it would most likely be for the Fe XVII line (or in the F-like Fe XVIII blend, which is used in the temperature diagnostic in Fig. 2, but which is not used in Fig. 3). Yet, the Fe XVII line appears to agree well with both the O VIII and Mg XI lines in all the panels of Figure 3 and in similar plots for the other spectra in our sample.

2. The ionization balance calculations could be incorrect. A complete answer to this question is outside the scope of this paper. However, the issue has been brought up recently only for iron, for which Arnaud & Raymond (1992) have revised the older calculations of Arnaud & Rothenflug (1985). In this paper we compare the results of the two calculations and find that neon varies in either case, while the iron, magnesium, and oxygen temperature-emission measure bands intersect for 24 of 33 cases for assumed standard abundances. (Note that we find the somewhat disconcerting result that, in those cases where "standard" abundances apply for the four lines, the Arnaud & Raymond ionization fraction gives somewhat better agreement of Fe XVII with the other three lines, while the temperature range of the intersection region of the four lines matches better with the Fe XVIII/Fe XVII line-ratio temperatures derived using Arnaud & Rothenflug ionization fractions. This suggests to us that the true ionization fractions might lie in between those given by the two calculations.)

3. The spectral line fluxes could be contaminated with other faint lines. The O VIII doublet is free from contamination, the Mg XI line has faint satellite lines which are resolved in the FCS spectra and their effects can easily be subtracted, and the Fe XVII line has no known contaminants at these low temperatures. It is well known, however, that the flux of the Ne IX line is contaminated by hot Fe XIX (and possibly Fe XVIII) lines during flares. Bhatia et al. (1989) analyzed FCS spectra of flaring plasma and compared these data with their predictions of iron lines. The main contaminating lines at 13.428 and 13.465 Å are present only during flares and there is no hint of them in the active region spectra used here. In addition, there are two small unresolved Fe XIX lines whose combined flux is certainly less than 5% of the Ne IX resonance line, a contribution smaller than the measurement error. There could also be contamination from as yet unidentified cool lines. However, it is not likely that this is the cause of Ne IX band deviation in Figure 3 because such contamination should affect all the spectra in the same way, including those depicted in Figures 3*a* and 3*b*.

4. There is a possibility of plasma variations with time during the 10 minutes it took for the FCS to scan the wavelength range and accumulate the spectrum. *Yohkoh* SXT image sequences show variations on timescales from minutes to days, even in quiescent active regions (Uchida et al. 1992; Shimizu et al. 1992). We took great care to eliminate spectra affected by such variations, by using the criteria discussed above in § 2 (also see discussion in § 3.3 below).

5. If the relative calibration across the wavelength range of the FCS were incorrect, the line fluxes would not be directly comparable: the Ne IX line at 13.45 Å is at the short-wavelength end of the first instrument channel, the Fe XVII line at 16.78 Å is in the center, and the O VIII line at 18.97 Å is at the long-wavelength end. The Mg XI line at 9.17 Å is scanned in another channel simultaneously with the O VIII line. It seems, however, that if the relative cali-

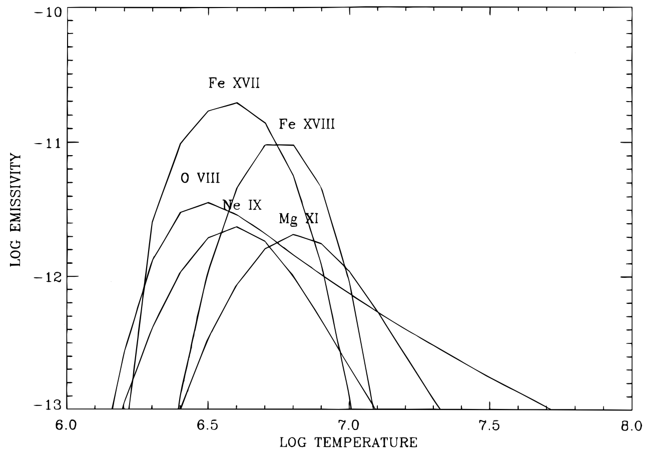


FIG. 4.—Emissivity plots from Mewe et al. (1985) for the five lines used in this analysis: Mg XI (9.17 Å), Ne IX (13.45 Å), Fe XVIII (14.22 Å), Fe XVII (16.78 Å), and O VIII (18.97 Å). Note that the Ne IX emissivity is embedded in among the other lines so additional high- or low-temperature plasma in the FCS field of view will affect these other lines preferentially.

bration were a problem, plots like those in Figure 3*a* and 3*b* (and 12 other spectra) could not be produced from the data. Further, a calibration problem could not produce both apparent enhancements and depletions of the neon flux.

6. If the spectral lines used here were not optically thin, opacity effects might masquerade as abundance variations. We refer to papers by Saba et al. (1996) and Schmelz et al. (1996) which show that the only spectral line in the FCS wavelength range significantly affected by resonance scattering is the Fe XVII line at 15.01 Å, which is not used in this analysis.

7. If the plasma were not effectively isothermal as we have assumed, an emission measure distribution could possibly mimic the abundance variations we observe. Qualitatively, we expect the fluxes of the other lines to be affected more strongly than that of Ne IX. This is shown in Figure 4 which plots the emissivities of the five lines used in this analysis from Mewe et al. (1985). Note that the Ne IX response is embedded in the middle of these lines, so hotter temperature plasma will affect the Fe XVIII and Mg XI lines preferentially, while cooler plasma will affect the O VIII line.

The most likely form of the emission measure for nonflaring active region plasma at these wavelengths (approximately 10–20 Å) is a distribution peaked around 2.5 to 3.5 million degrees and falling off steeply on either side (Raymond & Foukal 1982; Bruner et al. 1988; Brickhouse, Raymond, & Smith 1995). With this realistic version of the emission measure in mind, it is now easier to understand why the effectively isothermal approximation works in so many of the cases listed in Table 1. We are by no means saying that the plasma is truly isothermal, but rather that the plasma from quiescent active regions observed with our instrument (in our field of view, in our wavelength range, and in our 10 minute time window) is dominated by this $3 \times 10^6$ K plasma.

The most likely deviation from this distribution is expected to result from some form of heating, perhaps miniflaring of some loops in the field of view, which either broadens the emission measure distribution to higher temperatures or adds a separate high-temperature component (similar to the distribution obtained by differential emission measure analysis for flaring plasma). One of the main effects of such a distribution is the enhancement of high-temperature lines such as Mg XI which is used in this analysis and Fe XVIII at 14.22 Å. It is these lines, prominent in our quiescent spectra, that have the strongest high-temperature response and make the FCS instrument very sensitive to such temperature enhancements. All spectra with higher temperature lines like the Fe XIX lines near 13.5 Å were eliminated from the sample.

The question of an emission measure distribution is addressed more quantitatively in Tables 2, 3, and 4. In Table 2 we use the example of the spectrum taken on 1987 April 13 (number 6 in Table 1; Fig. 3*a*). This is a well-behaved spectrum with standard abundances. Initially, we assumed a flat emission measure distribution across the temperature

TABLE 2

EMISSION MEASURE DISTRIBUTION ANALYSIS: SPECTRUM NO. 6, 1987 APRIL 13

A. EMISSION MEASURE MODELS

| log $T$ | 6.20 | 6.30 | 6.40 | 6.50 | 6.60 | 6.70 | 6.80 | 6.90 | 7.00 | 7.10 |
|---|---|---|---|---|---|---|---|---|---|---|
| log EM1 ...... | 28.35 | 28.35 | 28.35 | 28.35 | 28.35 | 28.35 | 28.35 | 28.35 | 28.35 | 28.35 |
| log EM2 ...... | 28.35 | 28.35 | 28.35 | 28.35 | 28.35 | 28.35 | 28.35 | 0.00 | 0.00 | 0.00 |
| log EM3 ...... | 28.50 | 28.50 | 28.50 | 28.50 | 28.00 | 0.00 | 0.00 | 0.00 | 0.00 | 0.00 |
| log EM4 ...... | 0.00 | 28.00 | 28.90 | 28.90 | 28.00 | 0.00 | 0.00 | 0.00 | 0.00 | 0.00 |
| log EM5 ...... | 0.00 | 27.00 | 28.60 | 28.93 | 26.00 | 0.00 | 0.00 | 0.00 | 0.00 | 0.00 |

B. OBSERVED AND PREDICTED FLUXES

| Flux | O VIII | Ne IX | Mg XI | Fe XVIII |
|---|---|---|---|---|
| Flux Observed by FCS ...... | 53070 | 4677 | 874 | 2225 |
| Flux Uncertainty ............ | 4686 | 357 | 117 | 375 |
| Flux Predicted by EM1 ...... | 50705 | 4244 | 4024 | 18405 |
| Flux Predicted by EM2 ...... | 42777 | 3880 | 2328 | 15047 |
| Flux Predicted by EM3 ...... | 37584 | 2695 | 485 | 2281 |
| Flux Predicted by EM4 ...... | 73941 | 5327 | 914 | 3856 |
| Flux Predicted by EM5 ...... | 55590 | 4167 | 691 | 2667 |

TABLE 3

EMISSION MEASURE DISTRIBUTION ANALYSIS: SPECTRUM NO. 13, 1987 JUNE 13

A. EMISSION MEASURE MODELS

| log $T$ | 6.20 | 6.30 | 6.40 | 6.50 | 6.60 | 6.70 | 6.80 | 6.90 | 7.00 | 7.10 |
|---|---|---|---|---|---|---|---|---|---|---|
| log EM1...... | 28.35 | 28.35 | 28.35 | 28.35 | 28.35 | 28.35 | 28.35 | 28.35 | 28.35 | 28.35 |
| log EM2...... | 28.35 | 28.35 | 28.35 | 28.35 | 28.35 | 28.35 | 28.35 | 0.00 | 0.00 | 0.00 |
| log EM3...... | 28.50 | 28.50 | 28.50 | 28.50 | 28.00 | 0.00 | 0.00 | 0.00 | 0.00 | 0.00 |
| log EM4...... | 0.00 | 28.00 | 28.90 | 28.00 | 28.0 | 0.00 | 0.00 | 0.00 | 0.00 | 0.00 |
| log EM5...... | 0.00 | 27.00 | 28.60 | 28.80 | 26.00 | 0.00 | 0.00 | 0.00 | 0.00 | 0.00 |

B. OBSERVED AND PREDICTED FLUXES

| Flux | O VIII | Ne IX | Mg XI | Fe XVIII |
|---|---|---|---|---|
| Flux Observed by FCS ...... | 47519 | 1446 | 744 | 1493 |
| Flux Uncertainty ............. | 7029 | 156 | 438 | 504 |
| Flux Predicted by EM1...... | 50705 | 4244 | 4024 | 18405 |
| Flux Predicted by EM2...... | 42777 | 3880 | 2328 | 15047 |
| Flux Predicted by EM3...... | 37584 | 2695 | 485 | 2281 |
| Flux Predicted by EM4...... | 73941 | 5327 | 914 | 3856 |
| Flux Predicted by EM5...... | 45343 | 3312 | 534 | 2015 |

range of interest ($6.2 \leq \log T \leq 7.1$) and calculated the flux expected in four emission lines (O VIII, Ne IX, Mg XI, and Fe XVIII). We then compared these predictions with the observations and adjusted the input emission measure distribution to bring these into agreement. For the column emission measure distribution labeled EM1, we normalized (to log EM = 28.35; to determine the log of the volume emission measure, add 18.20 to the entries) so the observed and predicted Ne IX fluxes agreed within the 1 $\sigma$ measured uncertainty. This flat emission measure distribution produced acceptable fluxes for both the O VIII and Ne IX lines, but unacceptably high values for Mg XI and Fe XVIII. Therefore, in subsequent emission measure models EM2 and EM3, we dropped the high-temperature contribution and, in EM4 and EM5, dropped the low-temperature contribution. The resulting model, EM5, produced acceptable fluxes for all four lines. Note that it is very similar to the distributions found for the nonflaring Sun and Sun-like stars (Raymond & Foukal 1982; Bruner et al. 1988; Brickhouse et al. 1995).

Next, we tried the same type of analysis for a spectrum taken on 1987 June 13 (number 13 in Table 1; Fig. 3*c*) where the neon flux was low. The results are listed in Table 3. The emission measure distributions are the same as in Table 2 except that the fourth entry of distribution EM5 was lowered from 28.93 to 28.80. The fluxes of the O VIII, Mg XI, and Fe XVIII lines are within the measurement uncertainties for EM5, but that for Ne IX is not. Adding or subtracting high-temperature material will affect the Mg XI and Fe XVIII fluxes preferentially, while adding or subtracting cool material will affect the O VIII flux (Fig. 4).

Finally, in Table 4, we show the result of our attempts to reproduce the observed fluxes for the same spectrum (number 13 in Table 1; Fig. 3*c*) using a structured emission measure distribution such as that found for a weak active

TABLE 4

EMISSION MEASURE DISTRIBUTION ANALYSIS: SPECTRUM NO. 13, 1987 JUNE 13

A. EMISSION MEASURE MODELS

| log $T$ | 6.00 | 6.10 | 6.20 | 6.30 | 6.40 | 6.50 | 6.60 | 6.70 | 6.80 | 6.90 |
|---|---|---|---|---|---|---|---|---|---|---|
| log EM1...... | 28.20 | 28.50 | 28.60 | 28.50 | 28.30 | 28.20 | 28.30 | 28.20 | 27.80 | 27.20 |
| log EM2...... | 28.20 | 28.50 | 28.60 | 28.50 | 28.30 | 28.20 | 0.0 | 0.00 | 0.00 | 0.00 |
| log EM3...... | 28.90 | 28.50 | 28.60 | 28.50 | 28.00 | 28.00 | 28.30 | 0.00 | 0.00 | 0.00 |
| log EM4...... | 29.90 | 29.50 | 29.00 | 28.50 | 28.00 | 28.00 | 0.00 | 0.00 | 0.00 | 0.00 |
| log EM5...... | 30.50 | 30.00 | 29.50 | 28.50 | 27.50 | 28.10 | 0.00 | 0.00 | 0.00 | 0.00 |

B. OBSERVED AND PREDICTED FLUXES

| Flux | O VIII | Ne IX | Mg XI | Fe XVIII |
|---|---|---|---|---|
| Flux Observed by FCS ...... | 47519 | 1446 | 744 | 1493 |
| Flux Uncertainty ............. | 7029 | 156 | 438 | 504 |
| Flux Predicted by EM1...... | 35578 | 3047 | 1400 | 8926 |
| Flux Predicted by EM2...... | 22217 | 1398 | 170 | 541 |
| Flux Predicted by EM3...... | 23107 | 1893 | 465 | 2796 |
| Flux Predicted by EM4...... | 26115 | 2170 | 470 | 2796 |
| Flux Predicted by EM5...... | 32826 | 2785 | 415 | 2343 |

region by Brosius et al. (1996) using data from SERTS. Their distribution is reproduced in EM1 of Table 4, but does not result in fluxes that agree with the observed FCS values. Trying to increase the O VIII flux by artificially increasing the emission measure at low-temperatures results in failure because the O VIII response is falling off too quickly to contribute significantly. Therefore, we conclude that the apparent deficit in the neon abundance cannot be due to the presence of additional cool plasma to which the FCS is not sensitive. We also note that we did the same type of analysis for one of the spectra where the neon abundance was high (number 12 in Table 1; Fig. 3*e*) and got a similar result, i.e., the observed fluxes could not be reproduced with the emission measure models without adjusting the abundances.

None of these possibilities gives a satisfactory explanation for the Ne IX variations seen in Figures 1–3. Before concluding that these are abundance variations, however, we first investigate the isothermal approximation in more detail.

### 3.3. *The Effectively Isothermal Assumption*

In order to justify this "effectively isothermal" assumption and eliminate the possibility of high-temperature plasma in the FCS 15″ field of view, we have used four diagnostics from three separate instruments. These data are summarized in Table 1.

The low-intensity Fe XVIII line at 16.074 Å is in the FCS wavelength range, but is not always distinguishable from the background noise. It has a peak formation temperature of either 6.7 MK (Arnaud & Rothenflug 1985) or 7.0 MK (Arnaud & Raymond 1992) but, like most soft X-ray lines, has a broad temperature response so plasma considerably cooler than its peak temperature could contribute significantly to the line intensity. In column (7) of Table 1, a rating of "high" indicates that the line is clearly visible in the FCS spectrum and could be fitted easily with its own separate Voigtian profile; "medium" means that the line is distinguishable from the background noise, but might not be noticed if one were not looking for it; "low" indicates that the line is almost indistinguishable from the background noise; and "no" means that there was no hint of the line present.

Column (8) lists the maximum count rate (counts per second) in the Ca XVIII–XIX channel of the *SMM* Bent Crystal Spectrometer (BCS) recorded during the 60 minute daylight portion of the *SMM* orbit when the FCS spectroscopic scan was taken. The BCS observed the same region as the FCS, but had a 6′ (FWHM) field of view which observed the flux spatially integrated over the entire active region. Only spectroscopic scans where the BCS count rate was less than 60 counts $s^{-1}$ were included in Table 1. The background contamination, a result of a combination of cosmic rays and particles trapped in the Earth's radiation belts, generally varies between 3 and 7 counts $s^{-1}$. Any values above 10 are probably significant, but may not necessarily originate from within the 15″ FCS field of view. In some cases, the BCS data were not available. These times are indicated by the "NA" entries.

A "yes" in column (9) indicates that emission lines of the Ca XVIII–XIX line complex are visible in the BCS spectrum integrated over the entire 60 minute daylight portion of the spacecraft orbit. Once again, the emitting plasma may not necessarily have been in the FCS field of view. A "yes?" indicates that the lines were barely distinguishable from the noise while a "no" means that there were no lines visible. As above, "NA" indicates that the BCS data were not available.

*GOES*, the *Geostationary Operational Environmental Satellite*, has a full-disk X-ray monitor with a soft X-ray channel (1–8 Å) and a harder channel (0.5–4 Å). The information listed in column (10) indicates the highest level reached during that *SMM* orbit, using the standard *GOES* nomenclature for a logarithmic intensity scale. For example, the first entry "A5" indicates that the *GOES* background was stable at the A5 level, with an energy flux of $5 \times 10^{-8}$ W $m^{-2}$ in the soft X-ray channel. If there was an event, entry 4 for example, "B6*" indicates the highest level (an energy flux of $6 \times 10^{-7}$ W $m^{-2}$) achieved in the soft X-ray channel during the FCS spectral scan.

Clearly, the Fe XVIII line at 16.074 Å is the most relevant indicator since it responds only to high-temperature plasma in the FCS field of view, and it is this plasma which could affect the abundance analysis. However, this indicator must be calibrated, i.e., how strong can the line be and still not cause a problem with the "effectively isothermal" assumption? The data from the BCS and *GOES* are used in this determination. For example, all the listings in column (7) of "no" and "low" flux for the 16.074 Å Fe XVIII line have no significant entries in the BCS columns (where BCS data are available), except for numbers 12 (1987 May 29) and 29 (1987 December 15). Neither of these entries shows any hint of the 16.074 Å Fe XVIII in the FCS spectrum so we can be fairly confident that the hotter plasma was outside the FCS field of view. We can extrapolate these results to include those entries where the BCS data are not available.

There are two entries of "medium" Fe XVIII (16.074 Å) flux in column (7), for spectrum numbers 6 (1987 April 13) and 10 (1987 April 19). The emission measure versus temperature plot of the first is depicted in Figure 3*a* and shows no significant abundance variations. The plot for the second is similar, except that the emission measure is higher. We can conclude from these results that spectra with entries of "medium," "low," and "no" flux for the 16.074 Å Fe XVIII line in column (7) should not deviate significantly from the "effectively isothermal" assumption, and that there was no significant high temperature plasma in the FCS field of view.

The five entries of "high" Fe XVIII flux, however, suggest a different result. For these cases (numbers 8, 9, 11, 16, 27), all five BCS spectra show Ca XVIII–XIX lines, confirming that there is high-temperature plasma in the field of view, even if the event causing the enhanced temperature was not strong enough to show up in the *GOES* data. In several of these spectra, we may be picking up transient brightenings of the type described by Uchida et al. (1992) and Shimizu et al. (1992) for *Yohkoh* SXT image sequences. We exclude these spectra from further analysis where the "effectively isothermal" assumption is required. (Note: none of these spectra are used in Figs. 1–3.)

This analysis, together with that presented in the previous section, compels us to propose that both the neon abundance and the Ne/O abundance ratio varies in our sample of spectra. It is important to note that both enhancements and depletions with respect to the "standard" (Meyer 1985b) values are needed to explain the results. In the last column of Table 1, we list qualitative results of the abundance studies. Entries in this column marked with an asterisk denote spectra with evidence of hot plasma. Entries of "std" indicate that Ne/O for these spectra fell within measurement uncertainties of the standard value of 0.15. (Four values marked "std?*" indicate that Ne/O was consistent with being standard, but the spectrum also showed evidence of hot plasma which might compromise an isothermal analysis.) "Low" indicates that Ne/O was significantly lower than the standard value for seven cases (extreme cases are depicted in Fig. 3); for four of these cases (spectrum numbers 2, 3, 13, 14), it is clear that the neon abundance is low with respect to oxygen, magnesium, and iron. Six entries of "high" correspond to Ne/O abundance ratios higher than the standard value (extreme cases are illustrated in Figs. 3*e* and 3*f*); for three of these (spectrum numbers 20 [shown in Fig. 3*f*], 21, and 24), it is most plausible, based on the line-ratio temperature analysis, that the neon abundance is high relative to oxygen, magnesium, and iron. A question mark indicates that the results were inconclusive, or that two or more elements had abundances different from the standard values assumed.

A suggestive, but not conclusive, trend emerges from the analysis: the neon abundance seems to be relatively constant for a given active region, at least for a period of time. If the neon abundance of the region was found to be "high," "standard," or "low," later scans of that same region tend to have a similar abundance value, even though the FCS may have been pointed at a different location within the region. We note, however, that (1) not all of the spectra follow this rule and (2) all these spectra were obtained during the time of solar minimum when flare activity was infrequent. During a more active period, the variations may be significantly different.

## 4. DISCUSSION

Breneman & Stone (1985) and Meyer (1985a, 1985b) presented convincing evidence that coronal and photospheric plasmas were characterized by different sets of elemental abundances. The differences appeared to be based on the FIP of the element, with low-FIP elements enhanced by about a factor of 4 over high-FIP elements (Fig. 5). These results suggest a mechanism (or mechanisms) operating in the chromosphere where the low-FIP elements are essentially ionized while high-FIP elements remain predominately neutral. The early SEP review papers (Breneman & Stone 1985; Meyer 1985a) discussed abundances of the trace elements only with respect to each other, not relative to hydrogen. The single mention of hydrogen in the spectroscopy paper (Meyer 1985b) was based on *OSO 8* line-to-continuum measurements by Veck & Parkinson (1981). These measurements convinced Meyer (1985b) to conclude that the abundances of high-FIP elements were depleted in the corona with respect to their photospheric values while

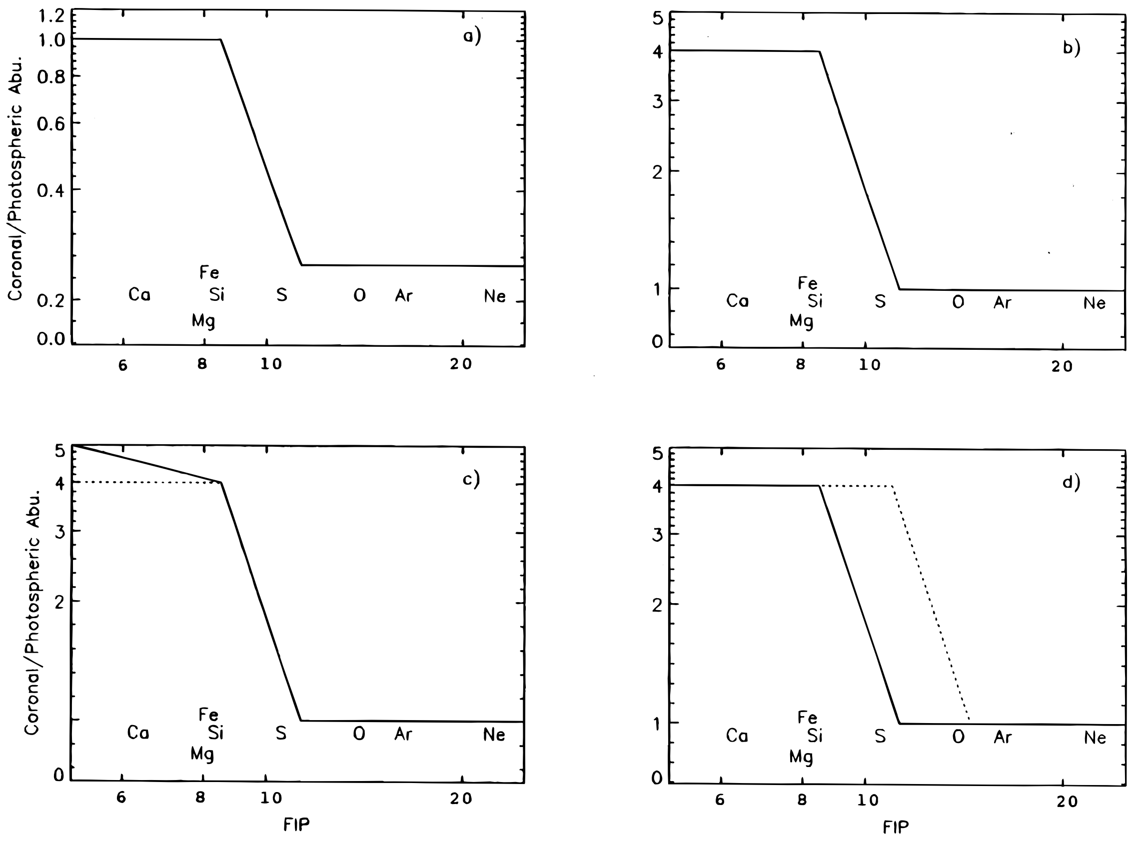


FIG. 5.—Schematic plots of the ratio of coronal to photospheric abundance of elements vs. their FIP for several scenarios. (*a*) The step-function distribution with the trace elements normalized with respect to silicon (low FIP) or with respect hydrogen where low FIP element abundances are the same in the corona and the photosphere, and high FIP elements are depleted with respect to their photospheric values (Meyer 1985b; Fludra & Schmelz 1995). (*b*) The step-function distribution where the trace elements are normalized with respect to oxygen (high FIP) or with respect to hydrogen, where low FIP elements are enhanced by a factor of 4 with respect to their photospheric values, and high FIP elements are the same in the corona and the photosphere (Feldman 1992; Meyer 1993). (*c*) The top step acquires a negative slope to account for enhanced values of the calcium abundance (Feldman 1992). (*d*) The step "slides" to the right to account for enhanced values of the sulfur and oxygen abundances (Feldman 1992).

those of low-FIP elements were the same in the corona and the photosphere (Fig. 5*a*). Vauclair & Meyer (1985) attempted to explain this fractionation with a gravitational diffusion mechanism. They computed the time required to deplete the upper atmosphere of neutral (high-FIP) elements, which are not inhibited by the assumed horizontal magnetic field which holds the ionized (low-FIP) elements in place. They found that the separation by gravitation alone is too slow and concluded that it is not an effective mechanism to explain FIP fractionation.

The work on coronal abundances that followed, reviewed in detail by Feldman (1992) and Meyer (1993), presented the FIP picture from a different perspective. The conclusion of these review papers was that the abundances of low-FIP elements were enhanced in the corona with respect to their photospheric values while those of high-FIP elements were the same in the corona and the photosphere (Fig. 5*b*). The theoretical work followed suit. The model developed by von Steiger & Geiss (1989) used a pressure gradient to drive a partially ionized plasma across vertically oriented magnetic field lines. The ions are trapped by the magnetic field for preferential transport to higher levels of the solar atmosphere. Although neutrals travel with the pressure gradient, they are unhindered by the magnetic field and are transported to the corona with their regular photospheric abundance.

Models have been proposed in which electromagnetic forces are used to drive the plasma across the magnetic field lines. Henoux & Somov (1993) suggest that the generation of currents flowing along magnetic flux tubes can provide two of the properties missing from the von Steiger & Geiss (1989) model. These internal currents and the azimuthal component of the magnetic field produce a radial force pointed inward which enhances the pressure in the flux tube via the pinch effect. In the photosphere, the density is high enough to couple the ions to the neutrals via collisions. In the chromosphere, however, the lower density effectively decouples the ions and neutrals, and the neutrals are able to move at velocities high enough to cross the field lines. The plasma transported to the corona is, therefore, rich with low-FIP elements, which were preferentially trapped.

Many observations seemed to confirm the basic FIP picture. But, as more was learned about coronal abundances, it was realized that a simple step function (Fig. 5*a* and 5*b*) based solely on a uniform low-FIP/high-FIP fractionation at a fixed threshold was too simplistic. Various manipulations of the FIP step function were suggested. For example, higher than expected values of calcium (FIP = 6.11 eV) relative to iron (FIP = 7.86 eV) observed in many flares (Veck & Parkinson 1981; Sylwester, Lemen, & Mewe 1984; Lemen, Sylwester, & Bentley 1986; Fludra et al. 1991, 1993; Sterling, Doschek, & Feldman 1993) could be explained by applying a negative slope to the top, low-FIP step (Fig. 5*c*; Feldman 1992). Anomalously low values of Ne/O (McKenzie & Feldman 1992) could result from shifting the entire step function to the right (Fig. 5*d*; Feldman 1992), so that oxygen behaved as an intermediate-FIP element. High values of sulfur (Fludra et al. 1993) could be "explained" with the same shift of the step-function threshold, which would group sulfur with the low-FIP elements.

Although the dominant abundance differentiation mechanism appears to be FIP-related, a second mechanism has sometimes been superposed to explain observed variations of elemental abundances. For example, during flares, chromospheric evaporation could mix FIP-biased coronal material with variable amounts of plasma from lower layers of the atmosphere which are characterized by "photospheric" abundances (Schmelz 1993; Antiochos 1994). This might explain all the available spectroscopic data where the calcium-to-hydrogen abundance ratio in flares is enhanced with respect to the photospheric value. Similarly, the variability of any low FIP element such as iron (Fludra et al. 1991) or intermediate FIP element such as sulfur (Fludra et al. 1993) might be accounted for with this combination of FIP differentiation and chromospheric evaporation. Recently, McKenzie & Feldman (1994) have considered another physical explanation for both the low-FIP abundance variations and the apparent shift in the low-FIP/high-FIP boundary, namely, a variable chromospheric ionization structure induced by photoionization. They argue that photoionization by blackbody radiation from just below the temperature minimum region, by locally produced Lyα radiation, could lead to variable enrichment factors of low-FIP elements, while photoionization of O I and other neutrals at the lower FIP end of the high-FIP species could shift the ion-neutral boundary, and thus the location of the step in coronal enhancement.

On the other hand, the variability of high-FIP elements such as argon (Veck & Parkinson 1982) and neon cannot be explained by either of these scenarios. An abundance differentiation mechanism based solely on low-FIP enhancement would require that the neon abundance does not vary at all (with respect to hydrogen). The first strong evidence to suggest that the neon abundance deviated from the photospheric value was reported for two very different solar flares observed by *SMM*: (1) Gamma-Ray Spectrometer observations of an X5 limb flare of 1981 April 27 (Murphy et al. 1991) and (2) FCS observations of an impulsive double flare on 1980 November 5 (Schmelz & Fludra 1993). In both cases, the neon abundance (relative to both high-FIP and low-FIP heavy elements) was higher than the expected coronal value. The combination of the FIP differentiation expected from SEPs and chromospheric evaporation could not explain the high neon abundances observed for these two flares or the high argon abundances observed by Veck & Parkinson (1982).

Another mechanism (or mechanisms) superimposed on the basic FIP differentiation model must be invoked to explain the enhanced neon or argon abundances. Shemi (1991) suggested that preflare soft X-ray radiation could penetrate deep into the solar atmosphere and create nonthermal ionization ratios at the base of the chromosphere. Because the photoionization cross section of neon (and argon) is high and the probability of recombination is low, ionized neon (and argon) could be selected along with the thermally ionized low-FIP elements for preferential transfer to higher levels of the solar atmosphere by the ion-neutral differentiating mechanism operating in the chromosphere. Therefore, the *interaction region*, i.e., the site of the plasma where the energetic particles and the ambient plasma interact during the flare, contains an overabundance of ionized neon (and argon) with respect to other elements with high FIP. Shemi (1991) emphasized that the process of building up the neon (and argon) ions in the low solar atmosphere takes time. If photoionization is responsible for the enhanced neon (and argon) abundance, there must be an extended period of energetic soft X-ray emission. This condition was met for both neon-enhanced flares: the 1981

April 27 flare was a long duration event which lasted several hours in soft X-rays and the 1980 November 5 flare had a long and intense preflare phase.

But the neon abundance variations in quiescent active regions described in this paper cannot be explained with photoionization by X-rays or chromospheric evaporation, since high-energy photons and energetic bulk plasma motions are not present in these regions. Since it is obvious from the analysis presented here that the abundance of neon varies, another (as yet unaccounted for) mechanism must combine with the FIP effects to explain the abundance variations. FIP is only part of the story of coronal composition.

## 5. CONCLUSIONS

In this paper, we present evidence that the elemental abundance of neon varies relative to the low FIP elements iron and magnesium and the high FIP element oxygen in quiescent active regions. There are several different indications of anomalous neon abundances in our sample of quiescent active-region spectra.

1. By visual inspection of spectra such as those shown in Figure 1, neon line intensities show larger than expected variability relative to both iron and oxygen lines.
2. In plots of line ratio versus temperature, Ne/Fe shows greater variability than Fe/O (Fig. 2), which argues for enhanced (and depleted) values of neon at least some of the time when Ne/O is anomalous.
3. In four spectra (numbers 2, 3, 13, 14 in Table 1), the single valid temperature-emission measure solution found from overlapping emission measure curves has the neon band depleted relative to the oxygen, magnesium, and iron bands; and
4. In three spectra (numbers 20, 21, 24 in Table 1), the more plausible (based on the line-ratio temperature analysis) of the two possible solutions found from overlapping emission measure bands had the neon band enhanced relative to oxygen, magnesium, and iron. Although in three other cases, a solution with oxygen depleted is equally plausible, all six cases imply Ne/O enhanced above the standard value, which is counter to the FIP scenario.

If we assume the "standard" coronal abundances listed in § 2 for oxygen, magnesium, and iron, our results imply neon variations in the range of $1.3 \times 10^{-5} \pm 15\% \leq \mathrm{Ne/H} \leq 7.5 \times 10^{-5} \pm 15\%$. (The FCS data by themselves cannot set or test the absolute abundance normalization relative to hydrogen. The derived abundances variations will scale with the normalization chosen.) We have used conservative criteria, discussed in § 3.3, to eliminate the possibility of significant high-temperature plasma in the FCS field of view during the spectroscopic scans used in this study. The plots in Figures 3*a* and 3*b* indicate that the isothermal approximation is justified for this analysis when we are careful to eliminate all but quiescent active region spectra. This assumption would certainly not be valid for flaring plasma and probably not for material in the decay phase of a long duration event. Meaningful results on elemental abundances from FCS spectra for such high temperature, dynamic plasma would require a (more complex) differential emission measure analysis (Schmelz 1993; Fludra & Schmelz 1995). For the quiescent active regions in our study, both energetic bulk plasma motions and high-energy photons seem unlikely to be sources of the observed abundance variations. The derived neon abundances tend to be fairly stable for a given active region, but this effect is not universal and the trend may not hold up during periods when the Sun is more active or for regions which are particularly flare productive. Abundance variations of the high-FIP element neon outside of flares have not yet been explained by any model seeking to predict coronal elemental abundances.

This work was supported by NSF grant ATM-9311834, a Cottrell Science Award from the Research Corporation, and NASA contracts NAS 5-28713, NAS 5-30431, and NASW-4814. It is a pleasure to thank M. Laming for helpful advice that made this a stronger paper, and J. C. Chauvin for assistance with data analysis.

## REFERENCES

Acton, L. W., et al. 1980, Sol. Phys., 65, 53
Antiochos, S. K. 1994, Adv. Space Res., 14, (4)139
Arnaud, M., & Raymond, J. 1992, ApJ, 398, 394
Arnaud, M., & Rothenflug, R. 1985, ApJS, 60, 425
Bhatia, A. K., & Doschek, G. A. 1992, Atomic Data Nucl. Data, 52, 1
Bhatia, A. K., Fawcett, B. C., Lemen, J. R., Mason, H. E., & Phillips, K. J. H. 1989, MNRAS, 240, 421
Breneman, H. H., & Stone, E. C. 1985, ApJ, 299, L57
Brickhouse, N. S., Raymond, J. C., & Smith, B. W. 1985, ApJS, 97, 551
Brosius, J. W., Davila, J. M., Thomas, R. J., & Monsignori-Fossi, B. C. 1996, ApJS, in 106, 143
Bruner, M. E., Haisch, B. M., Brown, W. A., Acton, L. W., & Underwood, J. H. 1988, J. Phys., Colloq. C1, Suppl. 3, 49, 115
Feldman, U. 1992, Phys. Scripta, 46, 202
Fludra, A., Bentley, R. D., Culhane, J. L., Lemen, J. R., & Sylwester, J. 1991, Adv. Space Res., 11(1), 155
Fludra, A., Culhane, J. L., Bentley, R. D., Doschek, G. A., Hiei, E., Phillips, K. J. H., Sterling, A., & Watanabe, T. 1993, Adv. Space Res., 13(9), 395
Fludra, A., & Schmelz, J. T. 1995, ApJ, 447, 936
Grevesse, N., & Anders, E. 1989, in AIP Conf. Proc. 183, Cosmic Abundances of Matter, ed. C. J. Waddington (New York: AIP), 1
Henoux, J.-C., & Somov, B. 1992, in Proc. First SoHO Workshop, ed. C. Mattock (ESA SP-348), 325
Lemen, J. R., Sylwester, J., & Bentley, R. D. 1986, Adv. Space Res., 6(6), 245
McKenzie, D. L., & Feldman, U. 1992, ApJ, 389, 764
———. 1994, ApJ, 420, 892
McKenzie, D. L., Keenan, F. P., McCann, S. M., Berrington, K. A., Hibbert, A., & Mohan, M. 1992, ApJ, 358, 378
Mewe, R., Gronenschild, E. H. B. M., & van den Oord, G. H. J. 1985, A&AS, 62, 197
Meyer, J.-P., 1985a, ApJS, 57, 151
———. 1985b, ApJS, 57, 173
———. 1993, Adv. Space Res., 13(3), 377
Murphy, R. J., Ramaty, R., Kozlovsky, B., & Reames, D. V. 1991, ApJ, 371, 793
Raymond, J. C., & Foukal, P. 1982, ApJ, 253, 323
Reames, D. V. 1995, Adv. Space Res., 15(7), 41
Saba, J. L. R., Schmelz, J. T., Bhatia, A. K., & Strong, K. T. 1997, in preparation
Saba, J. L. R., & Strong, K. T. 1991, ApJ, 375, 789
———. 1992, in Proc. First SoHO Workshop, ed. C. Mattock (ESA SP-348), 347
Saba, J. L. R., & Strong, K. T. 1993, Adv. Space Res., 13(9), 391
Schmelz, J. T. 1993, ApJ, 408, 373
Schmelz, J. T., & Fludra, A. 1993, Adv. Space Res., 13(9), 325
Schmelz, J. T., Saba, J. L. R., Chauvin, J. C., & Strong, K. T. 1997, ApJ, in press
Schmelz, J. T., Saba, J. L. R., & Strong, K. T. 1992, ApJ, 398, L115
Shemi, A. 1991, MNRAS, 251, 221
Shimizu, T.., Tsuneta, S., Acton, L. W., Lemen, J. L., & Uchida, Y. 1992, PASJ, 44, L147
Sterling, A. C., Doschek, G. A., & Feldman, U. 1993, ApJ, 404, 394
Strong, K. T. 1978, Ph.D. thesis, Univ. London

Strong, K. T., Claflin, E. S., Lemen, J. R., & Linford, G. A. 1988, Adv. Space Res., 8(11), 167
Strong, K. T., Lemen, J. R., & Linford, G. A. 1991, Adv. Space Res., 11(1), 151
Sylwester, J., Lemen, J. R., & Mewe, R. 1984, Nature, 310, 665
Uchida, Y., McAllister, A., Strong, K. T., Ogawara, Y., Tshimizu, Matsumoto, R., & Hudson, H. S. 1992, PASJ, 44, L155
Vauclair, S., & Meyer, J. P. 1985, in Proc. 19th Internat. Cosmic-Ray Conf., La Jolla, 4, 233
Veck, N. J., & Parkinson, J. H. 1981, MNRAS, 197, 41
von Steiger, R., & Geiss, J. 1989, A&A, 225, 222